Research article

Chitosan-olive oil microparticles for phenylethyl isothiocyanate delivery: optimal formulation

Ezequiel R. Coscueta[1,*], Ana Sofia Sousa[1], Celso A. Reis[2,3,4] and Manuela Pintado[1,*]

[1] Universidade Católica Portuguesa, CBQF - Centro de Biotecnologia e Química Fina – Laboratório Associado, Escola Superior de Biotecnologia, Rua Diogo Botelho 1327, 4169-005 Porto, Portugal
[2] i3S - Instituto de Investigação e Inovação em Saúde, Universidade do Porto, Porto, Portugal; celsor@ipatimup.pt
[3] Institute of Molecular Pathology and Immunology of University of Porto, Ipatimup, Porto, Portugal
[4] Medical Faculty, University of Porto, Al. Prof. Hernâni Monteiro, Porto, Portugal

* Corresponding authors
E-mail: ecoscueta@porto.ucp.pt (ERC); mpintado@porto.ucp.pt (MP)

Abstract: Phenylethyl isothiocyanate (PEITC), a chemopreventive compound, is highly reactive due to its considerably electrophilic nature. Furthermore, it is hydrophobic and has low stability, bioavailability and bioaccessibility, restricting its use in biomedical and nutraceutical or food applications. Thus, the encapsulation of this agent has the function of overcoming these limitations, promoting its solubility in water, and stabilizing it, preserving its bioactivity. So, polymeric microparticles were developed using chitosan-olive oil-PEITC systems. For this, an optimisation process (factors: olive oil: chitosan ratio and PEITC: chitosan ratio) were implemented through a central composite design. The responses were: the particle size, zeta-potential, polydisperse index, and entrapment efficiency. The optimal formulation was further characterized by FTIR and biocompatibility in Caco-2 cells. Optimal conditions were olive oil: chitosan and PEITC: chitosan ratios of 1.46 and 0.25, respectively. These microparticles had a size of 629 nm, a zeta-potential of 32.3 mV, a polydispersity index of 0.329, and an entrapment efficiency of 98.49%. We found that the inclusion process affected the optical behaviour of the PEITC, as well as the microparticles themselves and their interaction with the medium. Furthermore, the microparticles did not show cytotoxicity within the therapeutic values of PEITC. Thus, PEITC was microencapsulated with characteristics suitable for potential biomedical, nutraceutical and food applications.

Keywords: Phenethyl Isothiocyanate (PEITC); Microencapsulation; Chitosan nanocomposite; Olive Oil; Polymeric microparticle

1. Introduction

Phenylethyl isothiocyanate (PEITC) is released from the enzymatic hydrolysis of gluconasturtiin, the most abundant glucosinolate found in watercress (a vegetable from the family *Brassicaceae*) by the enzyme myrosinase [1]. Among all the isothiocyanates (ITCs), PEITC is one of the most extensively

studied with various biological activities such as antimicrobial [2], antioxidant and anti-inflammatory [3,4]. Several studies suggested that PEITC exhibits cancer preventive and therapeutic effects on multiple types of cancers [1,5–7] and is one of the ITCs that is being tested in clinical trials [8]. Although PEITC is biologically useful and has excellent potential as a health-promoting compound, its industrialization has been limited due to its relative volatility and instability [9]. PEITC is a highly reactive electrophile, which is susceptible to attack by nucleophilic molecules [4]. Furthermore, PEITC is a compound with low molecular weight (MW=163.2 g/mol) and considerable hydrophobicity (logP=3.47). Its pharmacokinetic feature includes first-order linear absorption with a high protein binding nature [10]. Therefore, its stabilization becomes a technological challenge. Cyclodextrin was reported as a plausible carrier for ITCs [11]. Besides, PEITC was already stabilized with vegetable oils, such as olive oil, once vegetable oil protects non-polar ITCs from decomposition or volatilisation [9]. Nevertheless, a relevant opportunity to stabilize PEITC and even increase its bioavailability in a nutraceutical matrix is microencapsulation.

Currently, methods of administration of bioactive compounds are increasingly sought in a selective, non-invasive way and with minimal side effects. Hence, microencapsulation is a technology used to improve the delivery strategy, promoting the controlled release and protect bioactive compounds, preserving their properties from undesirable reactions, while improving their functionality and bioavailability [12,13]. Additionally, polymeric microparticles gained significant importance as they are biodegradable, biocompatible and can be formulated using a sustainable approach [14]. In that sense, chitosan (CS) is biocompatible, biodegradable, and non-toxic, making it an ideal candidate as a biomaterial for biomedical applications, namely drug delivery systems [15,16]. CS is also mucoadhesive since it can establish connections between the charged groups from mucins. This property gives CS better selectivity at mucosal injured sites, where there is usually a higher expression of mucins, increasing its concentration at the site of absorption [17]. CS was also recognised by the United States Food and Drug Administration (US FDA) as Generally Recognised as Safe (GRAS), so its consumption is safe [18].

Microencapsulation is a strategy that has rarely been addressed as a way of administering PEITC or any ITCs [12]. Dharmala et al. developed a microparticle using stearic acid and chitosan to deliver PEITC, based on Solid Lipid Nanoparticle methodology. Their study demonstrated that Chitosan–SLN microparticles loaded with PEITC significantly improved the chemotherapeutic efficacy of PEITC [19]. These conclusions showed that PEITC can be stabilised by microencapsulation, a technique sparingly explored for ITCs so far. According to the few studies of microencapsulated ITCs, some methods seem more promising, mainly ionic gelation and complex coacervation. Both methods used chitosan, though are underexplored until now [12]. Currently, there is no study about the encapsulation of PEITC (or any ITCs), using chitosan and a liquid lipid, which opens a relevant research line aiming at identifying microparticles as delivery systems for bioactive compounds with potential use in biomedical and nutraceutical fields.

This work is part of a project that seeks to apply PEITC to treat ailments in the gastrointestinal tract (Fig 1). For this, it is necessary to design microparticle systems capable of releasing their content in response to a given stimulus. Specifically, the microparticles to be developed will be destined for the colon (Fig 1), so during their course, they must face a series of adverse conditions that result from the digestion

process, which are detrimental to PEITC in its free state. For this reason, this work aims to use CS as a polymer for the encapsulation of PEITC. On the other hand, it is also intended to give an even more innovative approach by combining CS with a liquid lipid, combining common use and good nutritional properties, such as olive oil (Fig 1). Finally, this work intends to select green techniques in the preparation of microparticles, minimizing the environmental impact and being as innocuous as possible for potential human use.

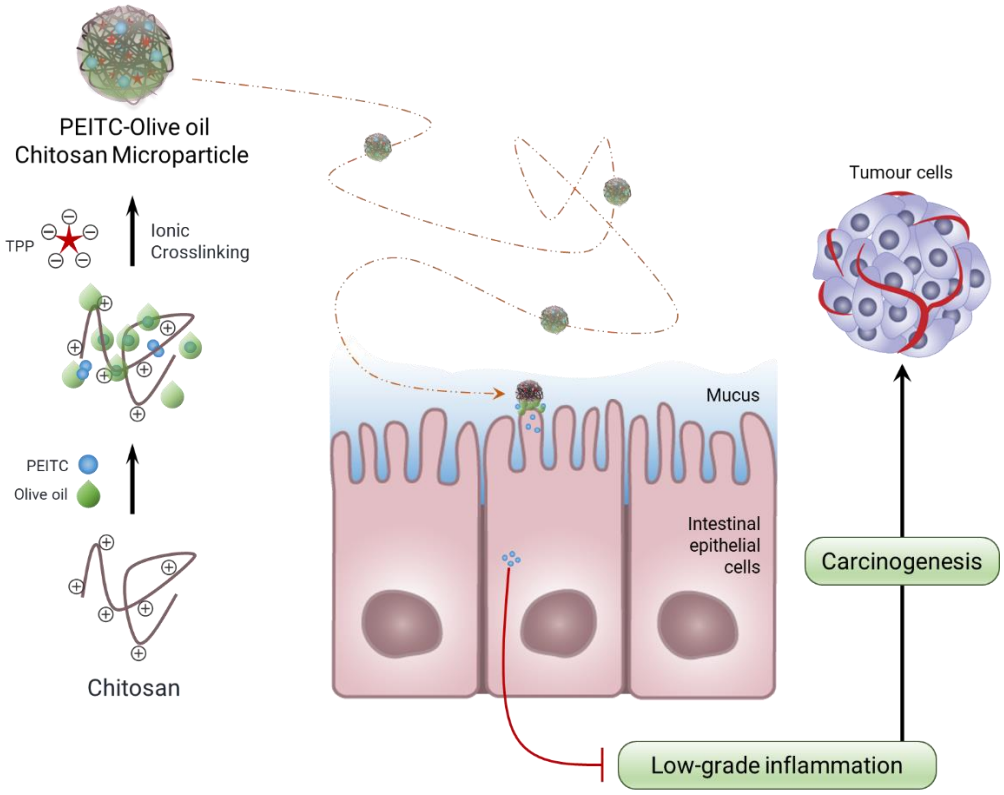

Fig 1. Overview of the great challenge. Representation of the global hypothesis that guides the specific objective of this initial development work.

2. Materials and Methods

2.1. Chemicals

Low molecular weight chitosan (CS) was obtained from Sigma-Aldrich (St. Louis, USA) and possessed a deacetylation degree between 75 and 85% and a molecular weight of 107 kDa. Sodium Tripolyphosphate (TPP) and MEM non-essential amino acid solution were supplied by Sigma-Aldrich (Merck, Darmstadt, Germany). Dulbecco's Modified Eagle Medium (DMEM) high glucose and Penicillin-Streptomycin mixture were obtained from Lonza (Basel, Switzerland). Fetal bovine serum (FBS) was purchased from Biowest (Nuaillé, France). All the reagents were used as received without further purification. PEITC standard was supplied by Santa Cruz Biotechnology Inc. (Dallas, Texas, USA). The olive oil was an extra virgin, purchased in a local store. All the other reagents were of analytical grade and used without further purification. Ultrapure water was used to prepare all the solutions.

2.2. Microparticle production

Microparticles (MPs) were produced using the ionic gelation methodology through adaptation of the procedure described by Madureira, Pereira, Castro and Pintado [20]. Briefly, CS was dissolved at 5 mg/mL in acetic acid 1%, dissolved for 72 h stirred at room temperature. For later use, the pH value was adjusted to 5 with NaOH. TPP was used at CS to TPP relation of 7:1. As MPs were produced, void ultra-pure water was used to preserve the working volumes previously described. In the case of PEITC-loaded CS MPs, the process began with the addition of 4 mL of CS and an amount of PEITC to maintain the PEITC: CS mass ratio of 0.5 to 1.0. The system was filled to 9 mL with ultra-pure water, which was then placed under gentle stirring and 1 mL of TPP were added, dropwise with a syringe pump, at room temperature. In the case of mixed PMs of CS and olive oil loaded with PEITC, the process was the same, but with the addition of olive oil before the addition of PEITC. In the case of optimisation experiments, the process remained the same but varying the proportions of the components, as described below. Now, for the validation experiment, the system was increased to a final volume of 30 mL, then increasing the volume to add CS, olive oil, PEITC and TPP.

2.3. Optimisation

An experimental strategy was implemented to reduce the number of experiments necessary to optimise the production of CS-olive oil MPs loaded with PEITC, as well as to establish the most influential factors. For this purpose, a 3-level (3^2) factorial experimental design was selected, which is a type of 3-level response surface design that includes a subset of runs of a full factorial at two levels. The factors evaluated were olive oil: CS mass ratio (X_A) and PEITC: CS mass ratio (X_B), and the selected responses variable (Y) were the particle size (as Z-average), zeta-potential, polydispersity index, and entrapment efficiency of PEITC. The design resulted in an arrangement of 9 treatments, which was executed in triplicate (a total of 27 runs) on successive days. The levels of the factors, coded as -1 (low), 0 (central point) and +1 (high), are shown in Table 1. To carry out the experiments, we proceeded as established in the exploratory analyses. Immediately after the production of each system, it was analysed, as described below.

Table 1. Levels for 2 experimental factors.

Factors	Levels		
	-1	**0**	**+1**
X_A [1]	0.00	1.25	2.50
X_B [2]	0.25	0.75	1.25

[1] Olive oil: CS mass ratio, [2] PEITC: CS mass ratio.

2.4. MPs characterization

2.4.1. Size, zeta-potential and polydispersity index

The MPs suspensions were analysed concerning their physical properties by dynamic light scattering (DLS). The measured parameters were particle size (Dh), polydispersity index (PdI) and zeta-potential (ZP). Size values for exploratory assays were determined based on intensity distribution by apparent hydrodynamic diameter. In the case of optimisation tests, as the correlation functions were monomodal, the cumulative analysis was applied instead of the distribution method, since it is a simple and robust procedure that does not make any assumption about the size distribution of the sample. The parameters obtained are the mean value for the size (Z-average) and the amplitude of the dispersion curve known as the Polydispersity Index (PdI). The Z-average is a calculated value of diameter based on the intensity and is comparable with other results only if the same scattering angle is used. Therefore, all the Dh values reported in the multifactorial analysis correspond to the Z-average values. The measurements were made at room temperature (25 °C) using a disposable folded capillary cell (Malvern, Worcestershire, UK), at a constant detection angle of 173 ° using the technology called NIBS (Non-Invasive Back-Scatter) that reduces the effect known as multiple scattering and the influence of contaminants in the sample. The Zetasizer NanoZSP photometric correlation spectrometer (Malvern Instruments Ltd., UK) was used, which allows the measurement of particle sizes between 0.6 nm and 6 µm. This equipment is equipped with a 10 mW He-Ne laser with an emission wavelength of 633 nm. Data were acquired and analysed using Zetasizer v. 7.11 software (Malvern Instruments Ltd., UK). All measures were performed in triplicate.

2.4.2. Determination of entrapment efficiency

The PEITC entrapment efficiency (EE) was determined by ultra-filtration centrifugation [21]. 4 mL of MP suspension was placed in a centrifugal filter unit (MWCO 10,000, Amicon® Ultra, Millipore, MA, USA) and centrifuged at 8,000 rpm for 1 h to separate the un-entrapped PEITC. 3 mL of the filtrate containing the free PEITC was concentrated by solid-phase extraction (SPE), using C_{18} Sep-Pak® cartridges (Waters Corporation, Milford, MA USA) with elution in vacuo, using 500 µLpure methanol as elution solvent. Following, the absorbance of the eluates was measured at 245 nm. The same amount of the diluted MP suspension was dissolved in methanol at 60 °C. The resultant sample was filtered through 0.45 µm-membranes and analysed for 245 nm absorbance. To determine the PEITC concentration, a calibration curve was constructed in methanol with PEITC concentrations of 0.2-6.6 mM. Measurements were made in 96-well Nunc UV transparent plate (Thermo Scientific, Waltham, MA, USA) with multidetection plate reader (Synergy H1, Vermont, USA) controlled by the Gen5 Biotek software version 3.04. The amount of PEITC entrapped in the MP was obtained by subtracting the free PEITC amount from the total PEITC amount in the suspension. The EE was calculated as follows:

$$\mathrm{EE}(\%) = \frac{PEITC_{entrapped}}{PEITC_{total}} * 100 \quad (1)$$

2.4.3. FTIR-ATR analysis

The spectra of empty and loaded MPs and pure PEITC was obtained with a Fourier transform infrared spectrometer (FTIR) (PerkinElmer Spectrum-100), with a horizontal attenuated total reflectance (ATR) accessory, with a diamond/ZnSe crystal. All spectra were acquired with 30 scans and 4 cm^{-1} resolution, in the region of 4000 to 600 cm^{-1}. Three replicates were collected for each sample. Spectrum corresponding to the medium (ultrapure water) was subtracted from the spectra of the MPs suspensions.

2.5. *In vitro* Biocompatibility

One cell line was considered throughout this work, namely, Caucasian colon adenocarcinoma cells—Caco-2 (ECACC 86010202). Caco-2 cells were maintained in DMEM high glucose supplemented with 10% (v/v) FBS, 1% (v/v) penicillin-streptomycin, and MEM non-essential amino acid solution. The culture was incubated at 37 ºC in a 5% (v/v) CO_2 humidified atmosphere. Cells were detached using TrypLE Express (Thermo Scientific, Waltham, MA, USA), seeded (1×105 cells/well) into 96 well Nunc Optical Btm Plt PolymerBase Black microplates (Thermo Scientific, Waltham, MA, USA), and incubated for 24 h. Afterwards, the culture media were carefully removed and replaced with empty MPs, PEITC loaded MPs and pure PEITC at different equivalent PEITC concentrations (38, 77, 153 and 306 µM for MPs; 51, 102, 204 and 408 µM for pure PEITC), all sterile filtered. After incubation for 24 h, the cytotoxicity of the samples was evaluated using the PrestoBlue™ HS Cell Viability assay (Thermo Scientific, Waltham, MA, USA), following the protocol described by the manufacturer. Fluorescence was measured using a fluorescence excitation wavelength of 560 nm and an emission of 590 nm by a microplate reader (Synergy H1, Biotek Instruments, Winooski, VT, USA). Cells in culture medium were used as a control, and wells without cells were used as blanks. The metabolic inhibition was determined according to the following Equation (2):

$$\%\ \text{Metabolic Inhibition} = \frac{F_{control} - F_{sample}}{F_{control}} * 100 \quad (2)$$

where $F_{control}$ and F_{sample} are the fluorescence intensities at 485 nm of control and sample, respectively. Six replicates for each condition were performed (n = 5).

2.6. Statistics

Each optimisation experiment was performed in triplicate and the results were expressed as the mean values with standard deviations (SD). For each response (Y), i.e. the previously explained responses from each treatment, the normal distribution of the residuals was determined by graphical analysis. Likewise, using the Durbin-Watson statistic, we verified for each model that the residuals did not present any significant correlation based on the order of the data. Then, the data were fitted to the following polynomial quadratic model:

$$Y = \beta_0 + \beta_A X_A + \beta_B X_B + \beta_{A,A} X_A^2 + \beta_{A,B} X_A X_B + \beta_{B,B} X_B^2 + \varepsilon \quad (3)$$

where X_A and X_B are the coded levels of the independent variables mentioned above; β_0, β_i, $\beta_{i,i}$ and $\beta_{i,j}$ are the regression coefficients for the independent term, the linear, quadratic and binary interaction effects respectively; and ε, the residual error [22,23]. The surface and contour graphs of the responses were generated from this model. The significance of the effects of each experimental factor in the model was estimated for each analysed response. The models were recalculated, considering only the significant effects, and thus obtained regression models with a good explanation of the data variability (R^2). Finally, a multi-criterion optimisation based on the Derringer's desirability function was applied [24] to the results of the experimental design, expressing the desirability of each response value on a scale of 0–1.

In the case of the validation test, a two-tailed hypothesis test relative to the difference between two sample means from normal distributions was applied for each response, considering a significance of 0.05 to reject the null hypothesis.

All statistical analysis was carried out with the aid of RStudio V 1.2.1335.

3. Results

3.1. Exploratory analysis

3.1.1. Effect of ultrasound homogenization

In this work, CS microparticles loaded with PEITC were formulated. Before expanding the formulation of these systems and their optimisation, we needed to set some technical parameters. As we intended to use ultrasound homogenization (UH), it was necessary to determine when to homogenize and then how much. Thus, we tried to produce the systems without ultrasound homogenization (without UH); with homogenization after ionic gelation (simple UH); and before and after ionic gelation (dual UH). In all cases, magnetic stirring was applied at high revolutions during the ionic gelation dripping. Fig 2 shows the distributions of the apparent hydrodynamic sizes (Dh) of the particles obtained in each condition. So, we saw that applying dual UH gave better results. Then, to continue, we evaluate the homogenization time, maintaining the intensity at 70% (parameter optimised in previous works). We tried homogenizing for 30 s, 45 s, 60 s and 120 s. We saw that it was more reproducible from 60 s. At 120 s, the system already acquired a very high temperature if it was not cooled. Therefore, we decided to establish the time of 60 s as a constant parameter of the process.

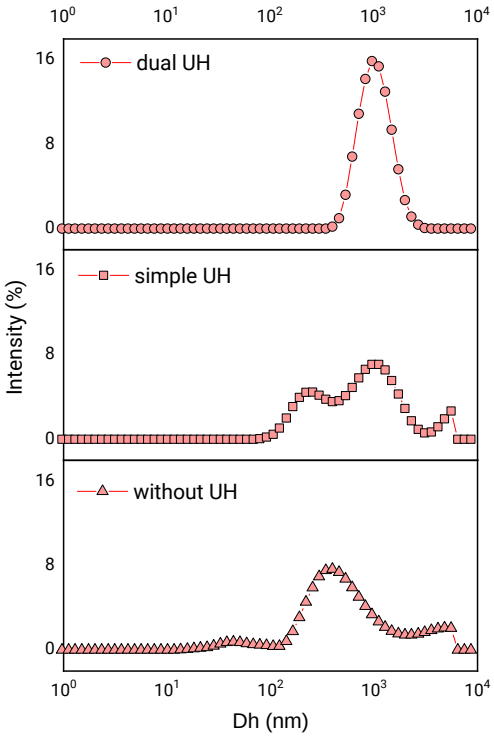

Fig 2. Effect of ultrasound. Distribution of apparent hydrodynamic diameters (Dh) according to the percentage of dispersion intensity, showing the effect of homogenization with ultrasound in the formation of CS microparticles. Results corresponding to the process with homogenized pre- and post-ionic gelation (dual UH); homogenized before ionic gelation (simple UH); without homogenized with ultrasound (without UH).

3.1.2. Effect of TPP flow rate

Another parameter to be analysed in the exploratory study was the drip flow of TPP in ionic gelation. For this, flows of 50, 100, 200 and 250 µL/min were tested to polymerise microparticles loaded with PEITC. Fig 3 shows the size distribution of the particles obtained in each condition. We saw that there were no appreciable changes in the distributions with increasing flow. However, due to the needle used for droplet formation, at a flow rate of 250 µL/min, some drops were projected out of the polymerization vessel due to the increased pressure of the syringe plunger. Therefore, a flow rate of 200 µL/min was chosen as a constant for all subsequent experiments.

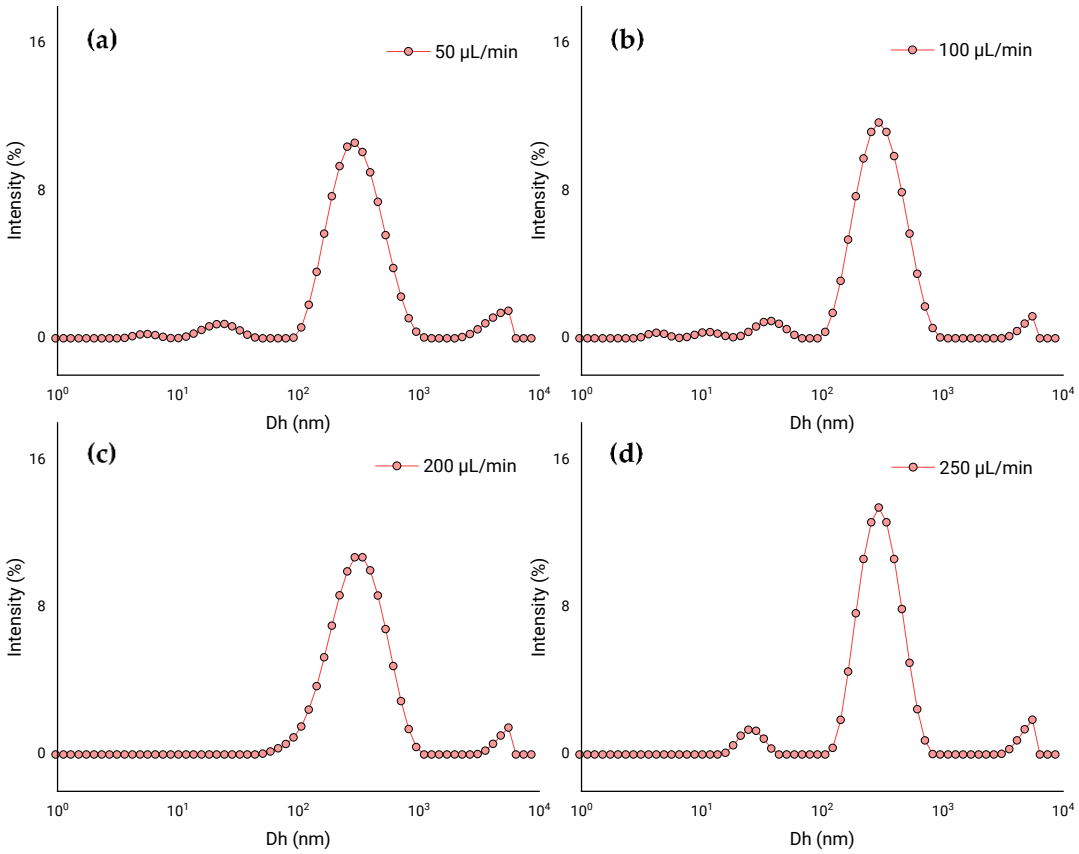

Fig 3. Effect of TPP dripping. Distribution of apparent hydrodynamic diameters (Dh) according to the percentage of dispersion intensity, showing the effect of the TPP flow rate on the ionic gelation of CS microparticles with PEITC. Results corresponding to the process with homogenization with ultrasound pre- and post-ionic gelation, and with a drop rate of TPP of 50 µL/min (**a**); 100 µL/min (**b**); 200 µL/min (**c**); 250 µL/min (**d**).

3.1.3. Incorporation of olive oil

Once the previous parameters were established, one of the factors to be studied in the subsequent optimisation was explored, the incorporation of olive oil in the formulation of the polymeric microparticles. CS microparticles were produced with olive oil in a ratio of 1.25:1.00 (olive oil: CS mass ratio): without PEITC and loaded with PEITC (0.50:1.00 PEITC: CS mass ratio). Fig 4 shows the particle size distributions in both conditions. As the graphs show, the incorporation of a liquid lipid such as olive oil improves the formation of polymeric microparticles loaded with PEITC. Furthermore, the system is better when both olive oil and PEITC are present (Fig 4a) than when PEITC is not loaded (Fig 4b).

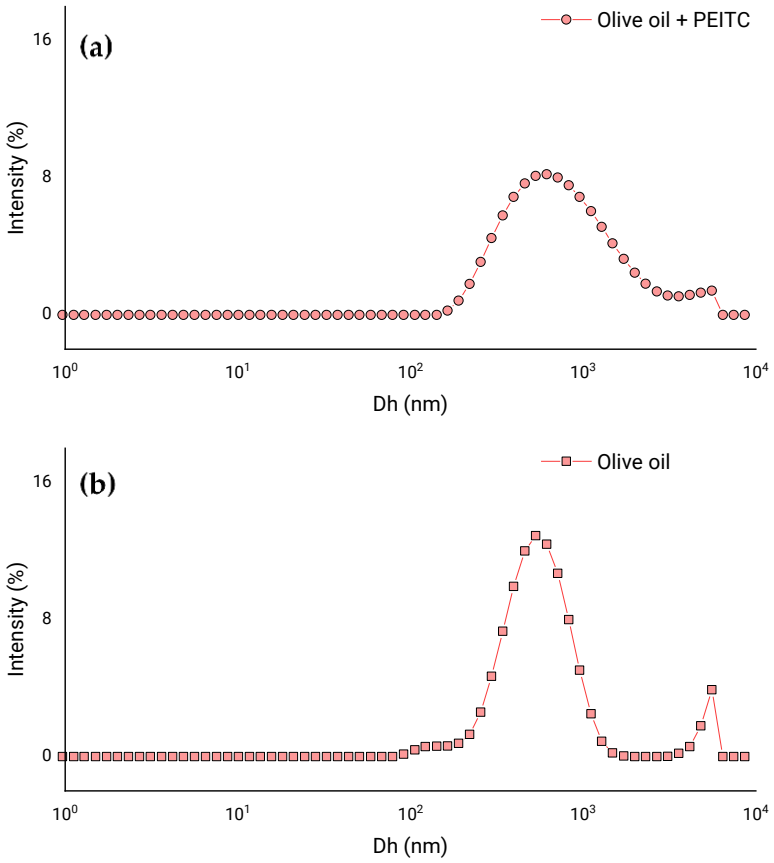

Fig 4. Effect of olive oil. Distribution of apparent hydrodynamic diameters (Dh) according to the percentage of dispersion intensity, showing the effect of the incorporation of olive oil in the formulation of CS microparticles loaded with PEITC. Results corresponding to the microparticles with a mass ratio of olive oil: CS of 1.25 to 1.00, with PEITC (**a**) and without PEITC (**b**).

3.2. Optimisation

Once the exploratory analyses have been completed, and the interest in producing hybrid microparticles (polymeric-lipid) with CS and olive oil to load PEITC has been established, we continue to develop an optimal model for our new system. Considering this, we selected an experimental design of the central composite type (described in section 2.3; see S1 Appendix for raw data and full analysis). We selected the factor levels considering that the important thing was the presence of PEITC, while the absence of olive oil would be considered. Table 2 shows the design matrix and the multiple regression results obtained for the 9 randomized treatments.

Table 2. Central composite factorial design for two factors and four responses.

Run	Factors		Responses †			
	X_A	X_B	Dh [1]	ZP [2]	PdI [3]	EE [4]
1	2.50	0.75	729 ± 19	10.6 ± 1.9	0.287 ± 0.014	99.46 ± 0.11
2	1.25	0.75	663 ± 3	22.1 ± 1.5	0.267 ± 0.009	99.55 ± 0.08
3	0.00	0.25	744 ± 87	33.7 ± 3.1	0.618 ± 0.042	98.21 ± 0.05
4	1.25	1.25	677 ± 18	13.2 ± 2.2	0.265 ± 0.002	99.65 ± 0.12
5	0.00	1.25	2222 ± 63	31.6 ± 1.5	0.299 ± 0.017	99.63 ± 0.08
6	2.50	1.25	735 ± 17	5.7 ± 0.1	0.274 ± 0.012	99.65 ± 0.04
7	0.00	0.75	1436 ± 194	37.5 ± 0.4	0.487 ± 0.016	99.44 ± 0.03
8	2.50	0.25	674 ± 40	19.8 ± 3.7	0.278 ± 0.008	99.08 ± 0.08
9	1.25	0.25	624 ± 5	32.3 ± 1.0	0.275 ± 0.010	98.70 ± 0.31

[1] Z-average diameter in nm, [2] zeta-potential in mV, [3] polydispersity index, and [4] entrapment efficiency in %. † Values expressed as mean ± SD of three replicates.

Fig 5 shows the Pareto charts with the contribution of the standardized effects of the model coefficients, for each response considered. Broadly speaking, we can say that in the case of the particle size (Fig 5a) and the polydispersity index (Fig 5c), the quadratic effect of the PEITC concentration was not significant, which could be neglected. In the case of the zeta-potential (Fig 5b), two coefficients did not have a significant effect on the response, both being quadratic coefficients. This means that the surface modelled for that response would have no curvature. For the entrapment efficiency (Fig 5d), the quadratic coefficient of the olive oil concentration did not have significance, thus it was negligible for the model.

Then, we recalculated the models, by eliminating the non-significant effects, with the criterion of maximizing the R^2_{adj}, fitting again from the multiple regression of the data. Table 3 shows the parameters of the final models, including the obtained regression statistics: R^2, R^2_{adj} and RSD. The new models adequately explain the variation in the response, with a maximum R^2_{adj}, all explaining more than 86% of the variability. Fig 6 shows the response surfaces of the final models, expressing the four responses as a function of the two considered factors.

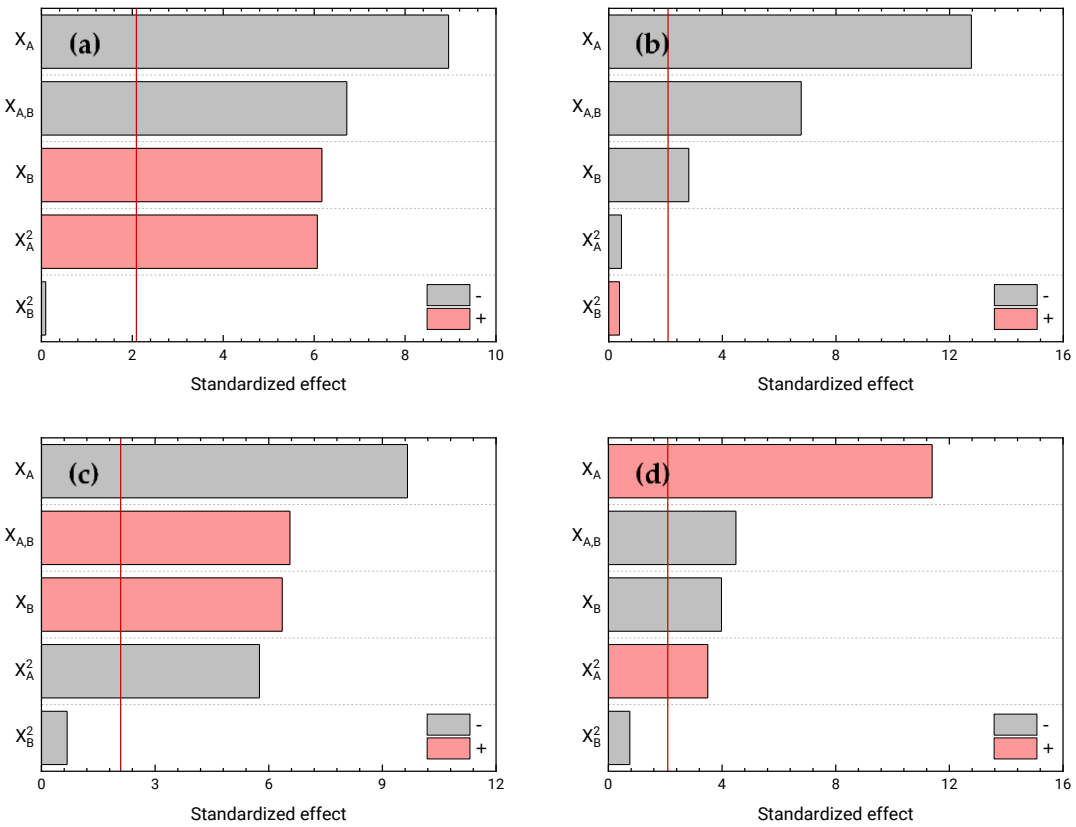

Fig 5. Pareto charts. Analysis of the effects of the central composite factorial design. Pareto charts with standardized effects of two experimental factors, in decreasing order of importance (in absolute value) for the Z-average diameter (**a**), zeta-potential (**b**), PdI (**c**), and entrapment efficiency (**d**). The vertical red lines represent the threshold of significance (P = 0.05) for 20 degrees of freedom.

Table 3. Estimates of the coefficients of each term in the recalculated model and the corresponding statistics.

Coefficient	Estimated coefficient values			
	Dh [1]	**ZP** [2]	**PdI** [3]	**EE** [4]
β_0	566.958	38.4027	0.669042	97.5416
β_A	-594.056	-5.28433	-0,337033	0.376989
β_B	1214.28	-578389	-0.2685	3.36528
$\beta_{A,A}$	281.778	-	0.0669511	-
$\beta_{B,B}$	-	-	-	-1.30556
$\beta_{A,B}$	-555.067	-4.812	0.126	-0.342
Statistics				
R^2	0.908	0.910	0.913	0.903
R^2_{adj}	0.891	0.899	0.898	0.885
RSD	173	3.559	0.040	0.170

[1] Z-average diameter, [2] zeta-potential, [3] polydispersity index, and [4] entrapment efficiency.

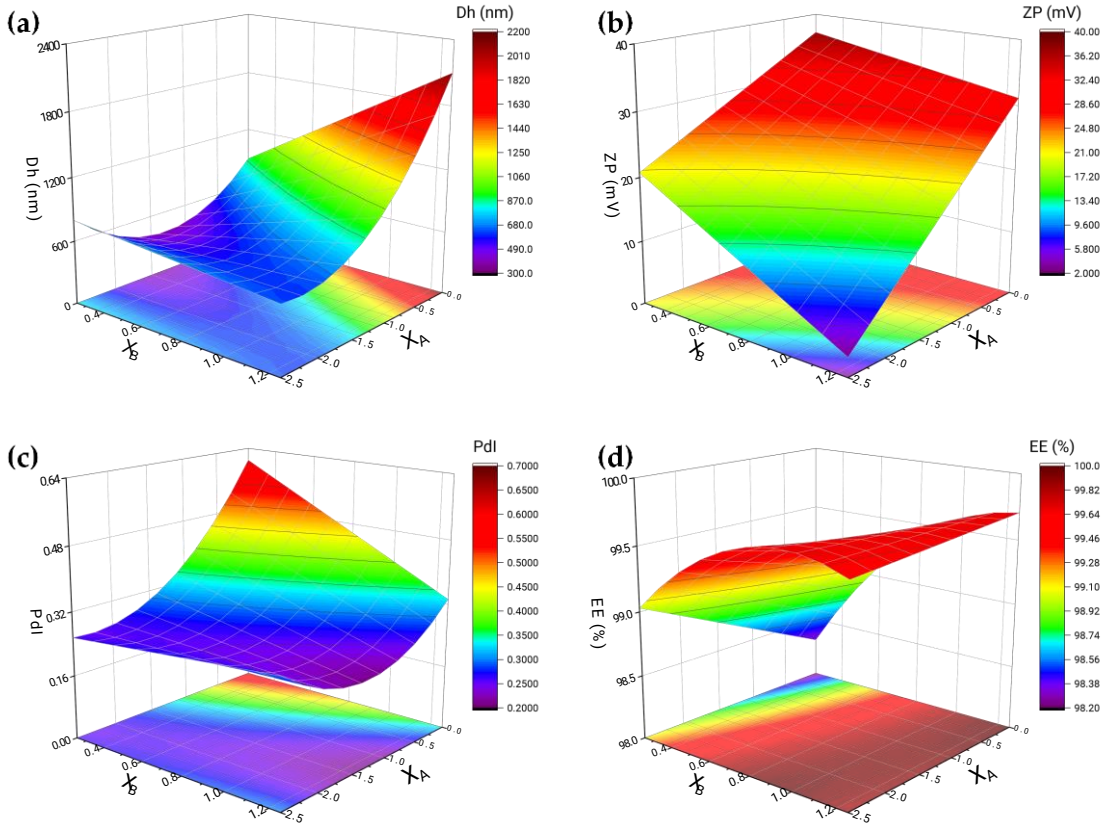

Fig 6. Response surfaces. Response surface models for the responses estimated based on two experimental. Charts for Z-average diameter (**a**), zeta-potential (**b**), PdI (**c**), and entrapment efficiency (**d**).

Fig 6a represents the response surface for the Z-average diameter. We see that the size of the particles produced grows towards maximum values of the PEITC content and minimum values of olive oil. This increase accelerates abruptly close to these limit values. At the same time, this size decreases with the decrease in the PEITC concentration, reaching its minimum at intermediate values of the range tested for the olive oil content. For its part, the zeta-potential (Fig 6b) increases, as expected, by decreasing the content of both hydrophobic compounds (PEITC and olive oil). As we already mentioned in the analysis of Pareto charts, this response surface is flat, so that, just as it reaches its maximum in one of its vertices, it reaches its minimum in another, at the maximum concentration values of PEITC and olive oil. In Fig 6c we see that the PdI reaches maximum values at minimum values of PEITC and olive oil. While at high concentrations of olive oil the PEITC concentration hardly affects the PdI, which is low, it reaches its minimum at high concentrations of PEITC and average values of olive oil. Finally, Fig 6d shows the response surface for entrapment efficiency. We see that the EE is minimal at low PEITC and olive oil values. This surface presents a marked curvature for the PEITC concentration, so it reaches almost maximum EE values already at intermediate values of the PEITC concentration range, beyond the olive oil concentration. However, the EE maximum is reached at the apex of the PEITC maximum and olive oil minimum. The desired optimisation for particle size and polydispersity index was minimization, while for the case of zeta-potential and entrapment efficiency it was maximization.

The optimal values for each response as well as the values of the factors for each of these optimal ones can be seen in Table 4. After the responses were optimised separately, they were optimised together based on the 'Derringer desirability' function. For this purpose, the goals of each of the responses were currently established as:

- Dh – minimize between 300-700 nm
- ZP - different from 0 mV
- PdI – minimize

EE was not considered for global optimisation, since it was not a determining factor since extremely satisfactory values were obtained in all experiments. Table 5 shows the combination of factor levels that maximizes the function of 'desirability' in the indicated region. This table also shows the predicted values for each response in that global optimal condition.

Table 4. Values of the factors that optimise each response and the corresponding predicted optimal response value.

Model	**Factor**		**Response** [3]
	X_A [1]	X_B [2]	
Dh	1.30	0.25	394
ZP	0.00	0.25	37.0
PdI	1.34	1.25	0.213
EE	0.00	1.25	99.71

[1] Olive oil: CS mass ratio, [2] PEITC: CS mass ratio. [3] Responses: dh (Z-average diameter) in nm; ZP (zeta-potential) in mV; PdI (polydispersity index) dimensionless; EE (entrapment efficiency) in %.

Likewise, Table 5 shows the result of the validation of the model as "observed". For this validation, the production test of the microparticles was carried out under the optimal conditions predicted but with additional complexity. The variability of increasing the volume of the reaction system by three times was added to the experiment, maintaining the same ultrasound probe as well as the same syringe and needle. Comparing the value of each response between predicted and observed with the hypothesis test, with a significance level of 0.05, we found no statistical differences, for which we were able to validate our model.

Table 5. Derringer optimisation of polymeric microparticles and validation.

Factor	**Low**	**High**	**Optimal**
X_A [1]	0.00	2.50	1.45
X_B [2]	0.25	1.25	0.25
Optimal desirability: 0.849			
Response [3]	**Optimal predicted** †		**Observed** †
Dh (nm)	400 ± 323		629 ± 50

ZP (mV)	27.6 ± 6.5	32.3 ± 1.75
PdI	0.300 ± 0.073	0.329 ± 0.040
EE (%)	98.72 ± 0.31	98.49 ± 0.09

[1] Olive oil: CS mass ratio, [2] PEITC: CS mass ratio. [3] Responses: Dh (Z-average diameter) in nm; ZP (zeta-potential) in mV; PdI (polydispersity index) dimensionless; EE (entrapment efficiency) in %. [†] Values expressed as mean ± SD of three replicates.

3.3. FTIR

Fig 7 shows the infrared spectra of the microparticles and pure PEITC. The characteristic peaks of the isosulphocyanic group (N=C=S) of PEITC [25] changed when incorporated into the microparticle. The respective bands of asymmetric and symmetric N=C=S stretching, changed from 2182 cm^{-1} and 2083 cm^{-1} to 2188 cm^{-1} and 2092 cm^{-1}, respectively in MP + PEITC. The low wavenumber shift revealed that the strength of the double bonds (N=C=S) was altered due to the occurrence of the inclusion action. A series of PEITC absorbance peaks disappeared or weakened with encapsulation as follows: -H stretch vibration at 3028 cm^{-1} in the benzyl group; bending vibration of -CH3 at 1454 and 1347 cm^{-1}; C-H plane bending vibration in benzyl around 700 cm^{-1}. A typical characteristic of the crosslinking between CS and TPP can also be seen in both MPs. Wu et al. [26] established that the peak at 1610 cm^{-1} of the bending vibration of –NH2, characteristic of CS, shifts to 1532 cm^{-1} in the polymerization between CS and TPP. In more recent work, Costa et al. [27] saw that same band at 1586 cm^{-1}. In our case, we saw this peak at 1555 cm^{-1} for MP, a shift perhaps due to the presence of olive oil. Furthermore, in the case of MP + PEITC, there was a smaller shift, at 1552 cm^{-1}, perhaps due to the inclusion of PEITC. We also found two bands related to the acetate in the medium [28,29]. The 1745 cm^{-1} (absorption peak of the carboxyl group) and 1416 cm^{-1} (δC-H vibrations of the CH3C=O residue) bands in the MP shifted to 1744 cm^{-1} and 1417 cm^{-1} in the MP + PEITC, respectively. In addition to displacement, there was a decrease in the intensity of the 1417 cm^{-1} band and an increase in the 1744 cm^{-1} band in MP + PEITC compared to MP. The increase in intensity to 1744 cm^{-1} implies an increase in the number of free acetate ions, while the intensity of the band related to the carboxyl salt (1417 cm^{-1}) decreases [30]. The results indicate that the electrostatic interactions between the carboxyl group of the acetate and the amino groups of the CS were altered with the inclusion of PEITC.

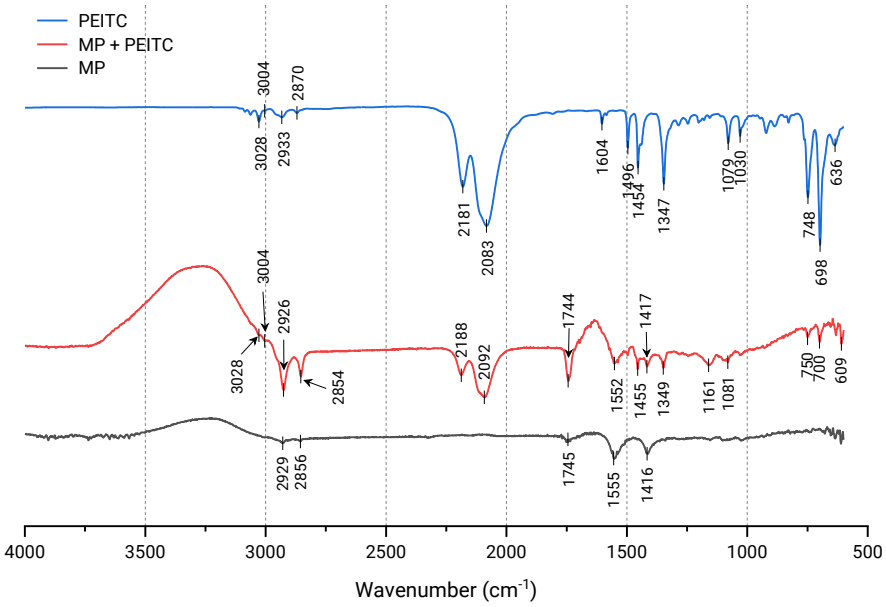

Fig 7. FTIR. Fourier transform infrared transmittance spectra for empty microparticles (MP), microparticles with PEITC (MP + PEITC) and pure PEITC.

3.4. Biocompatibility

The biocompatibility (or cytotoxicity) of the optimal microparticles with and without PEITC, as well as for pure PEITC, was analysed. For this, metabolic inhibition against Caco-2 cells was measured. According to the international standard ISO 10993-5 for the biological evaluation of medical devices (part 5: Tests for in vitro cytotoxicity), the threshold value for a sample to be cytotoxic is a metabolic inhibition of 30%. The results of the biocompatibility test were expressed as a function of the equivalent concentration of PEITC, given that although the empty microparticles did not present PEITC, they were diluted in the same proportion as those loaded with PEITC. As Fig 8 shows, pure PEITC at 408 µM was cytotoxic, while below 204 µM it had no cytotoxicity. In fact, below 102 µM the PEITC showed negative inhibition values, which could be due to the reported ability to stimulate antioxidant processes in the cell itself, increasing the reducing environment [31], which is precisely what the PrestoBlue assay directly measures. In the case of the microparticles without PEITC, they showed constant negative inhibition values despite the concentration, which may also be related to the reducing power of CS [32]. For the PEITC-loaded microparticles, cytotoxicity was already observed at the 153 µM PEITC concentration, while the inhibition values were negative below 77 µM. Thus, it turned out that encapsulated PEITC presented greater inhibitory power against Caco-2 cells than free PEITC.

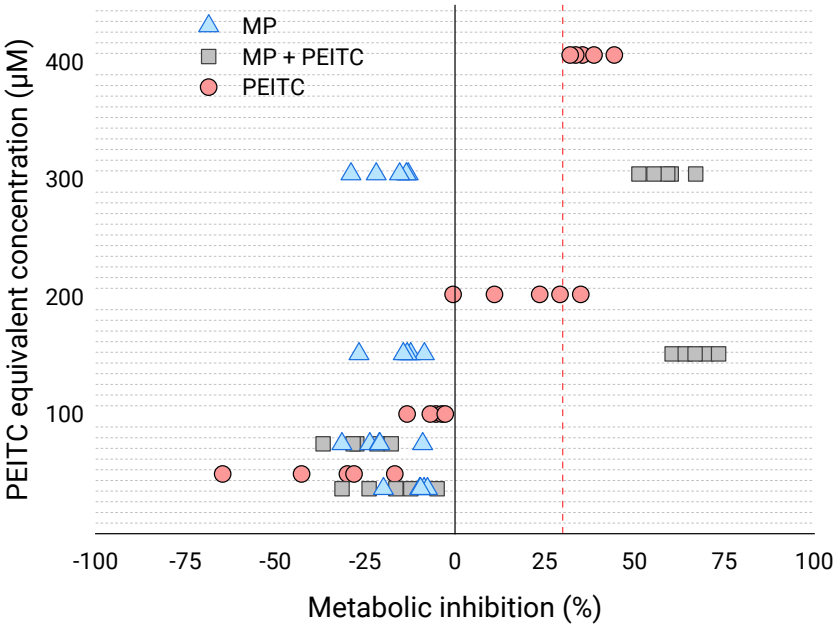

Fig 8. Biocompatibility. Metabolic inhibition of empty microparticles (MP), microparticles with PEITC (MP + PEITC) and pure PEITC at different equivalent concentrations of PEITC (38, 77, 153 and 306 µM for MP and MP + PEITC; 51, 102, 204 and 408 µM for pure PEITC) for 24 h against human colorectal adenocarcinoma Caco-2 cells. The scatter of independent determinations (n = 5) are represented. The dashed red vertical line represents the 30% inhibition limit.

4. Discussion

According to the National Nanotechnology Initiative, nanoparticles range from 1 to 100 nm. Meanwhile, the microparticles can vary between 100 and 10^5 nm. However, in pharmaceutical applications, the most common size varies between 100 and 1000 nm [33]. In order not to diffuse into the bloodstream or interstitial space and thus guarantee its arrival at the target site, the size of the MPs should not be less than 300 nm. In this sense, in this work, it was established that the ideal size of the MPs would be between 300 and 1000 nm. Therefore, it is essential to evaluate this parameter, to ensure that the MPs comply with the desired sizes since their dimensions interfere with the biodistribution, toxicity and bioavailability of the organism [17]. In the case of this study, this restriction was met by almost all the systems produced throughout the trials, highlighting this property for the case of the optimal system developed. With this, we can say that we obtained particles of satisfactory size.

Zeta-potential is an indicator that predicts the stability of microparticles in suspension, their tendency to aggregate, noting that particle aggregation compromises bioaccessibility to target sites [18]. This parameter expresses the potential difference at the interface of the surface of the MP and the solvent, so a zeta-potential between 20-30 mV guarantees moderate stability of the particles [15,20]. CS is a mucoadhesive polymer since its surface is full of positive charges. Therefore, the zeta-potential of MPs based on this polymer will be positive, indicating that, initially, the CS particles will be stable in suspension. Thus, the zeta-potential can predict the *in vivo* behaviour of these particles when they come into contact with biological media [13]. Furthermore, the zeta-potential can help to assess whether the PEITC is well

encapsulated within the particle or whether it was only adsorbed on the surface [34]. In our case, we observe that the zeta-potential decreases with the increase in PEITC and olive oil, with which part of it is adsorbed on the surface, but continues at more than acceptable values and, what is more, in the optimal system the value exceeds 30 mV. From this, it can be thought that the reticulated interior manages to create an even more hydrophobic and fluid environment with the presence of the liquid lipid. With this, we can say that we obtained particles not only with a satisfactory size but also stable and that they manage to incorporate both the lipid that acts as a copolymer and the compound to be loaded.

A priori, the ideal proportion of PEITC to add to the microparticles had to be tested based on the effectiveness of encapsulation, so it is known that as more PEITC is incorporated, after a certain point, and EE begins to decrease, possibly due to saturation of the microparticles [35]. However, in our case, we observed a very high EE in all cases. These high values probably did not correspond only to the trapped PEITC, but also to the adsorbed one, as we can see from the decrease in zeta-potential, given the great hydrophobicity of PEITC. Furthermore, we can reinforce this idea with FTIR analyse. The FTIR results indicate that the inclusion process affected the optical behaviour of the PEITC, as well as the MP itself and its interaction with the medium, which may point in the same direction as explained in the previous lines.

Knowing the dosages of a product is essential for its formulation since it is essential to know what quantities should be ingested for a specific purpose. On the other hand, these doses must first be biocompatible, that is, they must not present cytotoxicity. In a 2018 study, humans were given a dose of 40 to 80 mg PEITC/day orally for 30 days, with no adverse effects. However, when the consumed dose was increased to values between 120 and 160 mg of PEITC/day, during the same experimental period, some toxicity was observed [36]. In other studies, it was concluded that the acceptable daily dose is only 40 mg in humans, which is consistent with the previous study [5]. According to Abbaoui et al. [37], despite having some toxic effects on organisms, the dose for PEITC to exert its preventive and therapeutic effect is non-toxic and safe for humans. By analysing different reports, a range of PEITC performance values can be established from the most preventive phase to the most therapeutic phase, ranging from 5-30 μM, corresponding to 0.82 - 4.90 mg/L [1,38–43]. From our biocompatibility results, we can verify that the doses with therapeutic activity would be safe, both for free and encapsulated PEITC. Now, just as we saw that the toxicity of encapsulated PEITC was presented at lower concentrations than free, it remains to assess whether the same thing happens with preventive/therapeutic effectiveness. To do this, other parameters such as the PEITC release rate must first be analysed, as discussed in the next paragraph.

This work results in a novel advance in the matter of isothiocyanates as therapeutics. This is due to the novelty of encapsulating them, advancing technologically in preparation for possible biomedical and nutraceutical applications. This is a journey that is just beginning. What comes next? We still must analyse if our encapsulated compound is properly released, and if it is released how and how much. We must also analyse how encapsulation influences its bioactivities. Next, we must study the stability under gastrointestinal conditions. And finally, within our scope, to study whether CS improves the adhesion of these MPs and release in the lesion regions of the colon, where there is a greater expression of mucins.

References

1. Gupta P, Wright SE, Kim SH, Srivastava SK. Phenethyl isothiocyanate: A comprehensive review of anti-cancer mechanisms. Biochim Biophys Acta - Rev Cancer. 2014;1846(2):405–24 DOI: 10.1016/j.bbcan.2014.08.003.

2. Romeo L, Iori R, Rollin P, Bramanti P, Mazzon E. Isothiocyanates: An Overview of Their Antimicrobial Activity against Human Infections. Molecules. 2018;23(3):624 DOI: 10.3390/molecules23030624.

3. Moon PD, Kim HM. Anti-inflammatory effect of phenethyl isothiocyanate, an active ingredient of Raphanus sativus Linne. Food Chem. 2012;131(4):1332–9 DOI: 10.1016/j.foodchem.2011.09.127.

4. Kala C, Salman Ali S, Ahmad N, Jamal Gilani S, Ali Khan N. Isothiocyanates: a Review. Res J Pharmacogn. 2018;5(2):71–89 DOI: 10.22127/RJP.2018.58511.

5. Lam-Ubol A, Fitzgerald AL, Ritdej A, Phonyiam T, Zhang H, Myers JN, et al. Sensory acceptable equivalent doses of β-phenylethyl isothiocyanate (PEITC) induce cell cycle arrest and retard the growth of p53 mutated oral cancer in vitro and in vivo. Food Funct. 2018;9(7):3640–56 DOI: 10.1039/c8fo00865e.

6. Huong LD, Shim JH, Choi KH, Shin JA, Choi ES, Kim HS, et al. Effect of β-Phenylethyl Isothiocyanate from cruciferous vegetables on growth inhibition and apoptosis of cervical cancer cells through the induction of death receptors 4 and 5. J Agric Food Chem. 2011;59(15):8124–31 DOI: 10.1021/jf2006358.

7. Morris ME, Dave RA. Pharmacokinetics and pharmacodynamics of phenethyl isothiocyanate: Implications in breast cancer prevention. AAPS J. 2014;16(4):705–13 DOI: 10.1208/s12248-014-9610-y.

8. Dayalan Naidu S, Suzuki T, Yamamoto M, Fahey JW, Dinkova-Kostova AT. Phenethyl Isothiocyanate, a Dual Activator of Transcription Factors NRF2 and HSF1. Vol. 62, Molecular Nutrition and Food Research. Wiley-VCH Verlag; 2018. p. 1700908 DOI: 10.1002/mnfr.201700908.

9. Pusateri DJ, Kizer TR, Lowry AN. Extraction of non-polar isothiocyanates from plants. United States; US006824796B2, 2004.

10. Mohanty S, Sahoo AK, Konkimalla VB, Pal A, Si SC. Naringin in combination with isothiocyanates as liposomal formulations potentiates the anti-inflammatory activity in different acute and chronic animal models of rheumatoid arthritis. ACS Omega. 2020;5(43):28319–32 DOI: 10.1021/acsomega.0c04300.

11. Dagan ID, Frisbee AR, Newsome PW, Baudet MP. Stabilized sulforaphane. Vol. 1. United States; US007879822B2, 2011. p. 0–4 DOI: 10.1016/j.(73).

12. Zambrano V, Bustos R, Mahn A. Insights about stabilization of sulforaphane through microencapsulation. Heliyon. 2019;5(11) DOI: 10.1016/j.heliyon.2019.e02951.

13. Batista P, Castro PM, Madureira AR, Sarmento B, Pintado M. Recent insights in the use of nanocarriers for the oral delivery of bioactive proteins and peptides. Vol. 101, Peptides. Elsevier Inc.; 2018. p. 112–23 DOI: 10.1016/j.peptides.2018.01.002.

14. Mohammed MA, Syeda JTM, Wasan KM, Wasan EK. An overview of chitosan nanoparticles and its application in non-parenteral drug delivery. Pharmaceutics. 2017;9(4):53 DOI: 10.3390/pharmaceutics9040053.

15. Madureira AR, Pereira A, Pintado M. Current state on the development of nanoparticles for use against bacterial gastrointestinal pathogens. Focus on chitosan nanoparticles loaded with phenolic compounds. Carbohydr Polym. 2015;130:429–39 DOI: 10.1016/j.carbpol.2015.05.030.

16. Yuan Y, Chesnutt BM, Haggard WO, Bumgardner JD. Deacetylation of chitosan: Material characterization and in vitro evaluation via albumin adsorption and pre-osteoblastic cell cultures. Materials (Basel). 2011;4(8):1399–416 DOI: 10.3390/ma4081399.

17. da Silva SB, Ferreira D, Pintado M, Sarmento B. Chitosan-based nanoparticles for rosmarinic acid ocular delivery-In vitro tests. Int J Biol Macromol. 2016;84:112–20 DOI: 10.1016/j.ijbiomac.2015.11.070.

18. Batista P, Castro P, Madureira AR, Sarmento B, Pintado M. Development and characterization of chitosan microparticles-in-films for buccal delivery of bioactive peptides. Pharmaceuticals. 2019;12(1) DOI: 10.3390/ph12010032.

19. Dharmala K, Yoo JW, Lee CH. Development of Chitosan-SLN Microparticles for chemotherapy: In vitro approach through efflux-transporter modulation. J Control Release. 2008;131(3):190–7 DOI: 10.1016/j.jconrel.2008.07.034.

20. Madureira AR, Pereira A, Castro PM, Pintado M. Production of antimicrobial chitosan nanoparticles against food pathogens. J Food Eng. 2015;167:210–6 DOI: 10.1016/j.jfoodeng.2015.06.010.

21. Duong VA, Nguyen TTL, Maeng HJ, Chi SC. Nanostructured lipid carriers containing ondansetron

hydrochloride by cold high-pressure homogenization method: Preparation, characterization, and pharmacokinetic evaluation. J Drug Deliv Sci Technol. 2019;53(July):101185 DOI: 10.1016/j.jddst.2019.101185.

22. Myers RH, Montgomery DC. Response Surface Methodology : Process and Product Optimization using Designed Experiments. 2002. 798 p. DOI: 10.1080/00401706.1996.10484509.

23. Coscueta ER, Pellegrini Malpiedi L, Nerli BB. Micellar systems of aliphatic alcohol ethoxylates as a sustainable alternative to extract soybean isoflavones. Food Chem. 2018;264:135–41 DOI: 10.1016/j.foodchem.2018.05.015.

24. Derringer GC, Suich R. Simultaneous Optimization of Several Response Variables. J Qual Technol. 1980;12:214–9.

25. Yuan HN, Yao SJ, Shen LQ, Mao JW. Preparation and characterization of inclusion complexes of β-cyclodextrin-BITC and β-cyclodextrin-PEITC. Ind Eng Chem Res. 2009;48(10):5070–8 DOI: 10.1021/ie8015329.

26. Wu Y, Yang W, Wang C, Hu J, Fu S. Chitosan nanoparticles as a novel delivery system for ammonium glycyrrhizinate. Int J Pharm. 2005;295(1–2):235–45 DOI: 10.1016/j.ijpharm.2005.01.042.

27. Costa EM, Silva S, Vicente S, Neto C, Castro PM, Veiga M, et al. Chitosan nanoparticles as alternative anti-staphylococci agents: Bactericidal, antibiofilm and antiadhesive effects. Mater Sci Eng C. 2017;79:221–6 DOI: 10.1016/j.msec.2017.05.047.

28. Hasan MA, Zaki MI, Pasupulety L. Oxide-catalyzed conversion of acetic acid into acetone: An FTIR spectroscopic investigation. Appl Catal A Gen. 2003;243(1):81–92 DOI: 10.1016/S0926-860X(02)00539-2.

29. Ferri D, Bürgi T, Baiker A. Molecular interaction between cinchonidine and acetic acid studied by NMR, FTIR and ab initio methods. J Chem Soc Perkin Trans 2. 1999;(7):1305–11 DOI: 10.1039/a902514f.

30. Osman Z, Arof AK. FTIR studies of chitosan acetate based polymer electrolytes. Electrochim Acta. 2003;48(8):993–9 DOI: 10.1016/S0013-4686(02)00812-5.

31. Coscueta ER, Reis CA, Pintado M. Phenylethyl Isothiocyanate Extracted from Watercress By-Products with Aqueous Micellar Systems: Development and Optimisation. Antioxidants. 2020;9(698):1–11 DOI: 10.3390/antiox9080698.

32. Yen MT, Yang JH, Mau JL. Antioxidant properties of chitosan from crab shells. Carbohydr Polym. 2008;74(4):840–4 DOI: 10.1016/j.carbpol.2008.05.003.

33. Jóhannesson G, Stefánsson E, Loftsson T. Microspheres and nanotechnology for drug delivery. Dev Ophthalmol. 2015;55:93–103 DOI: 10.1159/000434693.

34. Gumustas M, Sengel-Turk CT, Gumustas A, Ozkan SA, Uslu B. Effect of Polymer-Based Nanoparticles on the Assay of Antimicrobial Drug Delivery Systems. In: Multifunctional Systems for Combined Delivery, Biosensing and Diagnostics. Elsevier; 2017. p. 67–108 DOI: 10.1016/b978-0-323-52725-5.00005-8.

35. Matshetshe KI, Parani S, Manki SM, Oluwafemi OS. Preparation, characterization and in vitro release study of β-cyclodextrin/chitosan nanoparticles loaded Cinnamomum zeylanicum essential oil. Int J Biol Macromol. 2018;118:676–82 DOI: 10.1016/j.ijbiomac.2018.06.125.

36. Chikara S, Nagaprashantha LD, Singhal J, Horne D, Awasthi S, Singhal SS. Oxidative stress and dietary phytochemicals: Role in cancer chemoprevention and treatment. Vol. 413, Cancer Letters. Elsevier Ireland Ltd; 2018. p. 122–34 DOI: 10.1016/j.canlet.2017.11.002.

37. Abbaoui B, Lucas CR, Riedl KM, Clinton SK, Mortazavi A. Cruciferous Vegetables, Isothiocyanates and Bladder Cancer Prevention. Mol Nutr Food Res. 2018;1800079 DOI: 10.1002/mnfr.201800079.

38. Soundararajan P, Kim J. Anti-Carcinogenic Glucosinolates in Cruciferous Vegetables and Their Antagonistic Effects on Prevention of Cancers. Molecules. 2018;23(11):2983 DOI: 10.3390/molecules23112983.

39. Giallourou NS, Rowland IR, Rothwell SD, Packham G, Commane DM, Swann JR. Metabolic targets of watercress and PEITC in MCF-7 and MCF-10A cells explain differential sensitisation responses to ionising radiation. Eur J Nutr. 2019;58(6):2377–91 DOI: 10.1007/s00394-018-1789-8.

40. Ramirez CN, Li W, Zhang C, Wu R, Su S, Wang C, et al. In Vitro-In Vivo Dose Response of Ursolic Acid, Sulforaphane, PEITC, and Curcumin in Cancer Prevention. AAPS J. 2018;20(1):19 DOI: 10.1208/s12248-017-0177-2.

41. Chen Y, Li Y, Wang XXX qi X qian, Meng Y, Zhang Q, Zhu J yun, et al. Phenethyl isothiocyanate inhibits colorectal cancer stem cells by suppressing Wnt/β-catenin pathway. Phyther Res. 2018;32(12):2447–55 DOI: 10.1002/ptr.6183.

42. Wang X, Govind S, Sajankila SP, Mi L, Roy R, Chung FL. Phenethyl isothiocyanate sensitizes human cervical cancer cells to apoptosis induced by cisplatin. Mol Nutr Food Res. 2011;55(10):1572–81 DOI:

10.1002/mnfr.201000560.

43. Dai M, Wang Y, Chen C, Li F, Xiao B, Chen S, et al. Phenethyl isothiocyanate induces apoptosis and inhibits cell proliferation and invasion in Hep-2 laryngeal cancer cells. 2016;1–8 DOI: 10.3892/or.